Back Door Modulation of the Farnesoid X Receptor: Design, Synthesis, and Biological Evaluation of a Series of Side Chain Modified Chenodeoxycholic Acid Derivatives

Roberto Pellicciari,*[,†] Antimo Gioiello,[†] Gabriele Costantino,[†] Bahman M. Sadeghpour,[†] Giovanni Rizzo,[§] Udo Meyer,[†] Derek J. Parks,[‡] Antonio Entrena-Guadix,[⊥] and Stefano Fiorucci[§]

Dipartimento di Chimica e Tecnologia del Farmaco, Università di Perugia, Via del Liceo, 1, 06123 Perugia, Italy, Dipartimento di Medicina Clinica e Sperimentale, Clinica di Gastroenterologia ed Epatologia, Università di Perugia, 06123 Perugia, Italy, GlaxoSmithKline Research & Development, Research Triangle Park, North Carolina 27709-3398, and Departamento de Quimica Farmacéutica y Orgànica, Facultà de Farmacia, Universidad de Granada, Campus de Cartuja s/n, 18071 Granada, Spain.

Received March 15, 2006

Carbamate derivatives of bile acids were synthesized with the aim of systematically exploring the potential for farnesoid X receptor (FXR) modulation endowed with occupancy of the receptor's back door, localized between loops H1−H2 and H4−H5. Since it was previously shown that bile acids bind to FXR by projecting the carboxylic tail opposite the transactivation function 2 (AF-2, helix 12), functionalization of the side chain is not expected to interfere directly with the orientation of H12 but can result in a more indirect way of receptor modulation. The newly synthesized compounds were extensively characterized for their ability to modulate FXR function in a variety of assays, including the cell-free fluorescence resonance energy transfer (FRET) assay and the cell-based luciferase transactivation assay, and displayed a broad range of activity from full agonism to partial antagonism. Docking studies clearly indicate that the side chain of the new derivatives fits in a so far unexploited receptor cavity localized near the "back door" of FXR. We thus demonstrate the possibility of achieving a broad FXR modulation without directly affecting the H12 orientation.

Introduction

The farnesoid X receptor (FXR, NH4R1) is emerging as a particularly attractive target[1] within the family of nuclear receptors, not only for the promising therapeutic potential associated with its modulation but also because of some peculiar features relative to ligand recognition by its ligand binding domain (LBD) that have emerged from crystallographic studies. Thus, while initially identified as a transcriptional sensor for bile acids being the primary bile acid chenodeoxycholic acid (CDCA, **1**, Chart 1), the most potent endogenous ligand,[2−4] FXR is now emerging as a key modulator of a variety of metabolic processes and might be involved in the etiology of human diseases. In particular, because of the availability of selective and potent FXR agonists, such as GW4064 (**2**), fexaramine (**3**), and 6-ECDCA (INT747, **4**) (Chart 1),[5−7] the recent identification of a subset of genes regulated by FXR activation has allowed the uncovering of an elaborate FXR-regulatory cascade for the maintenance of cholesterol and bile acid homeostasis,[8−10] and has suggested the potential existence of crosstalk between bile acid metabolism, triglyceride metabolism, and insulin resistance.[11−14]

These important findings have demonstrated that FXR may represent a valuable therapeutic target for the management of several diseases including liver disorders, hyperlipidimia, and obesity. Selective FXR modulators (referred to as "selective bile acid receptor modulators", SBARMs, in analogy with the well-known "selective estrogen receptor modulators", SERMs) are therefore particularly sought in view of their conceptual ability to activate (or repress) an individual gene or a cluster of genes without affecting the others, thus reducing the pleiotropism of FXR's action. In this context, the analysis of some of the features that have emerged from the crystallization of three holo forms of the LBD of FXR is of particular interest because they provide the molecular and structural basis toward the design of novel SBARMs. In particular, with retention of the common and conserved architecture of most nuclear receptors, consisting of a bundle of 12 α-helices,[15] the LBD of FXR shows peculiarity in terms of ligand recognition.[16] Thus, the potent bile acid agonist 6α-ethyl-chenodeoxycholic acid (6ECDCA, INT-747, **4**)[5] is bound to LBD with ring A directed toward H11−H12, while the carboxylic acid function of the side chain approaches the entry pocket at the back. This disposition is different from that adopted by other cholesterol metabolites that bind to their cognate receptors with the oxidized tail toward H12.[17] Furthermore, ring A is not directly in contact with the crucial H12 but rather stabilizes its "active" disposition through a triad of residues W466 (H12), H444 (H11), and Y358 (H10). Intriguingly, the bile acid agonists did not directly interact with members of the triad but provided the correct disposition of the partner residues through steric restriction of the H444 mobility.[16] A third peculiarity became apparent from the inspection of one of the X-ray structures of holo-LBD, which is the presence of two GRIP-2 peptides. Indeed, many LBDs of nuclear receptors have been cocrystallized with short peptides containing the LxxLL sequence of coactivators, but only in the case of FXR (1OSV, chain B) two peptides could be cocrystallized bound in an antiparallel fashion. Whether this observation is due to crystallographic artifacts or is of functional/physiological relevance is still an open question, but it has been proposed that the enhanced coactivator recruitment of FXR might have a mechanistic role. Along this line, by in silico screening, we have recently identified a possible second binding pocket in the FXR-LBD which can be in contact with the second coactivator cleft.[18]

Taken together, all of the above evidence delineates an intriguing scenario where the possibility of modulating the transactivation properties of FXR from the back of LBD does

* To whom correspondence should be addressed. Phone: +39 075 585 5120. Fax: +39 075 585 5124. E-mail: rp@unipg.it.

[†] Dipartimento di Chimica e Tecnologia del Farmaco, Università di Perugia.

[§] Clinica di Gastroenterologia ed Epatologia, Università di Perugia.

[‡] GlaxoSmithKline Research & Development.

[⊥] Universidad de Granada.

10.1021/jm060294k CCC: $33.50
Published on Web 06/15/2006

Chart 1. Natural and Synthetic FXR Agonists

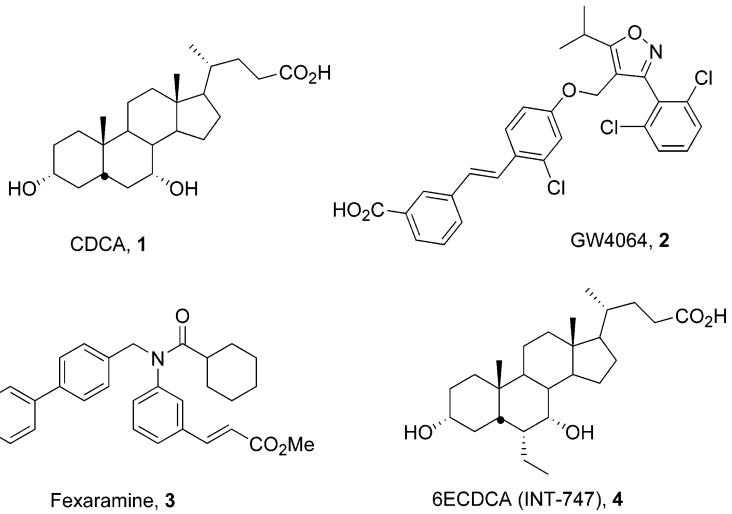

Chart 2. 3α,7α-Dihydroxy-24-nor-5β-cholan-23-amine Derivatives

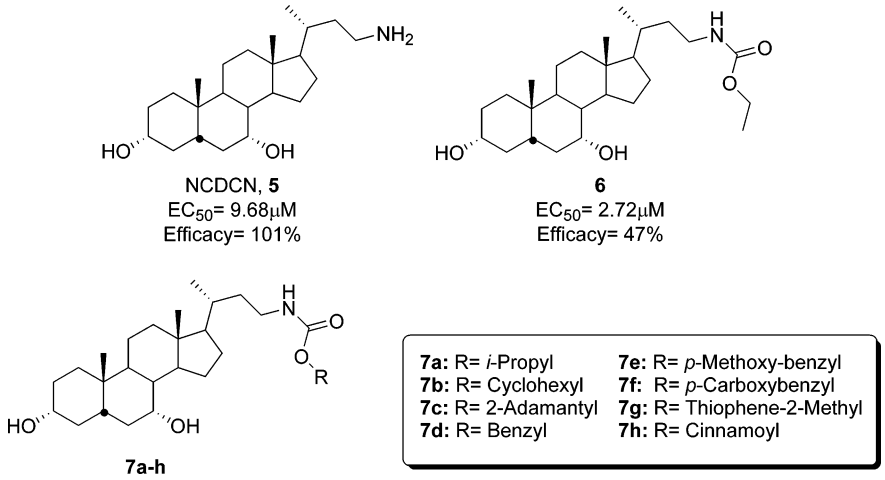

exist. In particular, we were fascinated by the observation that the carboxylic side chain of bile acids is projecting opposite the transactivation function 2 domain (AF-2), localized into H12, and potentially interacting with the binding cleft for the second coactivator. Support to this idea also comes from our recent work showing that modulation of FXR activity could be achieved by a small modification in the side chain.[19] Now, we have undertaken a more focused study, where a series of side chain modified analogues of CDCA are synthesized and evaluated as FXR modulators in both cell-free and cell-based assays. The results will be discussed with the help of systematic docking experiments.

Design Strategy

We have previously shown that the substitution of the distal carboxylic acid group of CDCA (**1**) by an amino group (NCDCN, **5**) preserved both the affinity and the efficacy of the parent derivative CDCA (**1**).[19] Furthermore, we showed that carbamoylation of **5** afforded the corresponding ethylcarbamate derivative **6**, which was 3-fold more potent than **5** but endowed with an efficacy of 47%, thus displaying the profile of a partial agonist (Chart 2).[19] In an attempt to rationalize this result, the X-ray structure of the LBD of rat FXR complexed with 6ECDCA (PDB code: 1OSV)[16] was selected for molecular modeling studies. Chain A of 1OSV was used after removing water molecules and the cocrystallized SRC-1 peptide. Then, inspection of the Connolly surface of the complex between LBD and **4** revealed the presence of a clearly defined binding pocket of about 190 Å^3 localized just above the carboxylate tail of 6ECDCA (**4**), projecting toward the cleft between H1−H2 and H5, and encompassed by residues belonging to H1, H3, H4, and H7 (Figure 1).

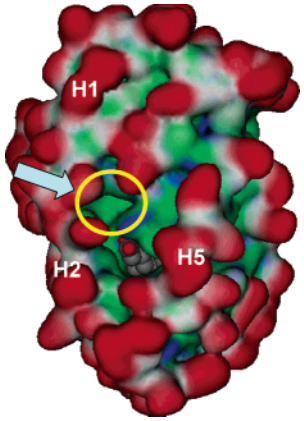

Figure 1. Connolly accessible surface of LBD complexed with 6ECDCA (INT-747, **4**). The cyan arrow indicates the ∼ca. 190 Å^3 wide additional binding pocket just above the carboxylate tail of **4** (represented as a space-filled model). The positions of helices H1−H2 and H5 are also indicated.

In this paper, we report the exploitation of this newly identified additional binding pocket through the preparation of

Scheme 1. Parallel Solution-Phase Synthesis for the Construction of the Focused Carbamate CDCA Analogues Small Library[a]

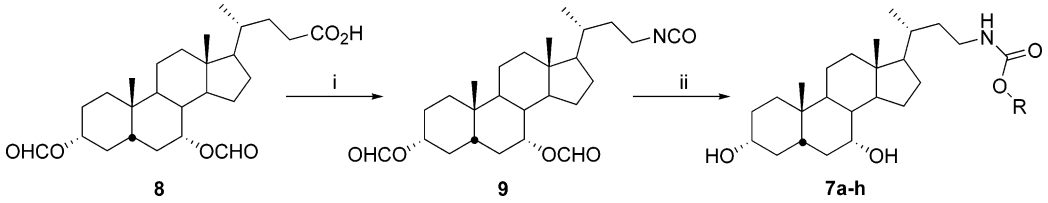

[a] (i) (a) $(SOCl)_2$, reflux; (b) NaN_3, H_2O, acetone, room temp; (c) toluene, reflux; (ii) (a) ROH, toluene, reflux; (b) K_2CO_3, MeOH, room temp.

an array of 3α,7α-dihydroxy-24-nor-5β-cholan-23-amine derivatives (**7a**−**h**) as new ligands for the FXR receptor (Chart 2). In these derivatives, the carboxylic tail of CDCA (**1**) was substituted by a carbamate moiety and the newly generated distal 26 position was scanned by the introduction of groups characterized by different steric, electrostatic, and hydrogen-bonding profiles. It should be mentioned that the 24-nor-5β-cholan-23-amine nucleus was already exploited for the preparation of reverse amide analogues of conjugated bile acids.[20]

Chemistry

A parallel solution-phase chemistry approach was chosen for the construction of the focused carbamate CDCA analogues small library (Scheme 1). 3α,7α-Diformyl-CDCA (**8**)[21] was converted into the corresponding acyl azides by treatment of the acyl chloride intermediate with aqueous sodium azide. The crude acyl azide mixture was then refluxed in dry toluene for 5 h to give the corresponding isocyanate **9** via Curtius rearrangement. With a carousel apparatus, intermediate **9** was reacted in toluene with diverse alcohols (see Table 3) to obtain the corresponding 3α,7α-diprotected CDCA carbamate analogues, which after basic hydrolysis with potassium carbonate in methanol gave the desired compounds **7a**−**h** in good yields.

Results

Fluorescence Resonance Energy Transfer (FRET) Based Coactivator Assay. To determine whether the newly synthesized compounds could promote the association of FXR with coactivators in vitro, the molecules were tested in a cell-free ligand-sensing assay using FRET to measure the ligand-dependent recruitment of the steroid receptor coactivator-1 (SRC-1) to FXR.[6] The FRET ligand-sensing assays were run in the presence of increasing concentrations of compounds to determine the half-maximal effective concentration (EC_{50}) and the maximal response in the recruitment of SRC-1 peptide (efficacy). The two steroidal FXR agonists CDCA (**1**) and 6ECDCA (**4**) were used as control ligands. Inspection of the results reported in Table 1 indicated that all compounds showed a significant increase in affinity with respect to CDCA (**1**), but in general they did not reach the maximum effect, thus displaying the profile of partial agonists. Only compounds **7e** and **7f** showed an efficacy similar to that of CDCA (**1**).

Cell-Based Luciferase Assay. To further investigate the FXR-activating properties of the new derivatives **7a**−**h**, we performed a cell-based luciferase assay. Thus, HepG2 cells were cotransfected with a FXR response element carrying a luciferase reporter plasmid and expression vectors for FXR and RXR together with a pCMV-β-galactosidase control vector. Cells were exposed to vehicle alone, to CDCA (20 μM), and to compounds **7a**−**h** (20 μM). Activation of luciferase reporter gene was measured in relative light units with β-galactosidase activity as a control for transfection efficiency and presented as normalized luciferase units. Inspection of the transient transfection assays revealed that all compounds were full agonists or partial agonists of FXR (Figure 2) with the exception of **5** (3% of transactivation relative to CDCA) and **7c** (3%), which did not transactivate, and of compound **7h** (10%) which retained only a weak transactivation activity. In contrast, compounds **7a** (120%) and **7g** (133%) were more potent than CDCA (**1**). **7b**, **7d**, **7e**, and **7f** can be considered as partial agonists in this assay with transactivation activity relative to CDCA of 27%, 41%, 40%, and 62%, respectively.

Table 1. Binding Potency and Efficacy of the Semisynthetic 3α,7α-Dihydroxy-24-nor-5β-cholan-23-amine Derivatives to FXR

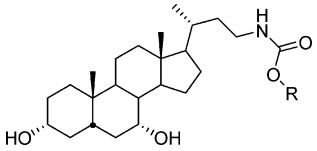

Comp.d	Trivial Name	R	EC_{50} (μM)	Efficacy (%)[a]
1	CDCA		8.66	100
4[5]	6ECDCA (INT-747)		0.098	144
5[19]	NCDCN		9.68	101
6[19]		Ethyl	2.72	47
7a			2.50	61
7b			1.14	77
7c			0.60	43
7d			0.79	62
7e		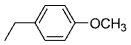	1.48	106
7f		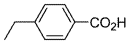	7.11	98
7g			0.41	63
7h		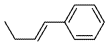	0.59	66

[a] Relative recruitment of the SRC1 peptide to FXR. Efficacy calculated relative to CDCA (**1**).

To further characterize the profile of compounds **5**, **7c**, and **7h**, a transactivation assay was carried out for these compounds in the presence of CDCA (**1**). Figure 3 shows that compounds **5**, **7c**, and **7h** inhibited the transactivation activity of CDCA (**1**), thus ruling out the possibility that the lack of transactivation was due to their inability to cross the cell membrane. Hence, compounds **5**, **7c**, and **7h** can be considered as FXR antagonists.

Docking Analysis. Docking experiments were performed on the carbamate derivatives **6** and **7a**−**h** in an attempt to clarify their binding modes and the molecular basis of their functional profiles. Thus, the X-ray structures of chain A and chain B of the LBD of the rat FXR complexed with 6ECDCA (pdb code: 1OSV) were selected. As previously reported, the two chains

Table 2. Docking Results for the Semisynthetic 3α,7α-Dihydroxy-24-nor-5β-cholan-23-amine Derivatives

	no. of clusters		more populated cluster[a]		type of complex[b]		binding energy (kcal/mol)	
compd	chain A	chain B	chain A	chain B	chain A	chain B	chain A	chain B
6	10	6	1st	1st	I	I	−12.22	
			2nd		II		−12.10	
7a	10	18	1st	1st	II	I	−12.70	−14.41
			2nd	2nd	I	II	−12.38	−14.09
7b	18	23	1st	1st	I	I	−14.40	−16.48
			2nd	2nd	II	II	−13.98	−15.87
			3rd		AAA		−14.37	
7c	29	44	1st	1st	I	I	−16.64	−18.06
			2nd	2nd	II	II	−15.29	−17.53
			3rd	11th	II	BBB	−15.51	−14.18
			4th		I		−15.64	
			8th		BBB		−13.68	
7d	19	15	1st	1st	II	I	−15.00	−17.69
			2nd		I		−14.61	
7e	35	23	1st	1st	II	I	−14.63	−17.13
			2nd		I		−14.32	
			3rd		II		−13.93	
			4th		III		−13.96	
7f	35	25	first	1st	II	I	−14.78	−17.98
			3rd		I		−14.59	
			5th		III		−14.07	
7g	18	19	1st	1st	II	I	−13.67	−16.23
			2nd		I		−13.57	
			3rd		III		−13.22	
7h	12	10	1st	1st	I	I	−14.89	−17.49
			2nd	2nd	II	II	−14.76	−16.48
			4th		II		−14.47	
			5th		III		−14.24	
			6th		III		−13.97	

[a] First more populated cluster containing a given type of complex (I, II, III, AAA, or BBB). [b] Type of complex observed in the first more populated cluster.

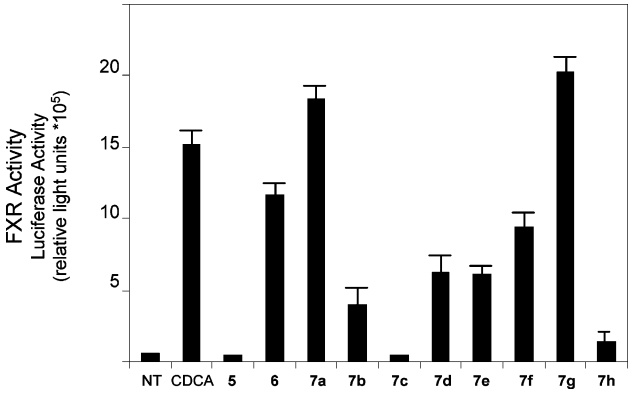

Figure 2. FXR-activating property of the new derivatives in a luciferase assay. Cells were exposed to 20 μM of each compound. Luciferase activity was normalized using β-gal as the internal control. Relative luciferase expression in untreated cells (NT) is shown.

Table 3. Alcohol Used in the Carbamoylation Reactions and the Corresponding Yields

compd	alcohol	yield (%)
7a	2-propanol	64
7b	cyclohexanol	73
7c	2′-adamantol	69
7d	benzyl alcohol	70
7e	*p*-methoxy-benzyl alcohol	75
7f	methyl 4-(hydroxymethyl)benzoate	70
7g	thiophene 2-methanol	65
7h	cinnamyl alcohol	72

differ in that in chain B there are two bound coactivator peptides while only the "canonical" one is cocrystallized with chain A. The presence of the second ("noncanonical") peptide might have functional relevance, and as recently pointed out by us, it influences the conformation of the receptor in proximity of loop H1−H2.[22] Since the additional binding pocket for the extended

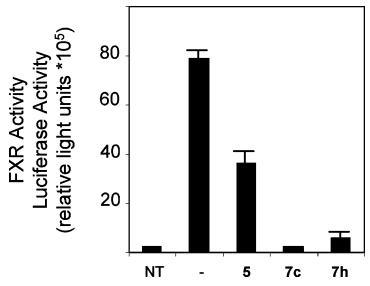

Figure 3. FXR-activating ability of CDCA alone and in combination with **5**, **7c**, or **7f** in a luciferase assay. Cells were exposed to 20 μM of CDCA and 20 μM of each studied compound. Luciferase activity was normalized using β-gal as the internal control.

side chains of compounds **6** and **7a**−**h** is localized in the proximity of loop H1−H2, docking experiments were carried out simultaneously on both chains in order to investigate the impact of this conformational variability. Water molecules, the coactivator peptides, and the agonist 6ECDCA (**4**) were removed from the crystal structures, and docking experiments were performed with Autodock 3.0 as described in the methods section.

Inspection of the docking results, reported in Table 2, revealed the occurrence of three slightly different nonequivalent dispositions that we call complexes I, II, and III, respectively. It is interesting to note that complex III is only present in chain A, where the absence of the second coactivator peptide makes a larger space for the extended side chains of **7a**−**h**. In both chain A and chain B, the most stable dispositions always correspond to complex I or to complex II, and in all the cases, the docking disposition of the steroidal skeleton almost exactly reproduces the crystallographically determined disposition of the skeleton of 6ECDCA (Figure 4).[16]

As far as the side chain is concerned, in both complex I and complex II the distal tail is projected into the newly described additional binding pocket lined by residues Arg328, Ile 332 (H5); His291, Ile294, Leu 295, Phe 298 (H3); Tyr 257 (H1); and Met 262 (loop H1−H2). The only difference between complex I and complex II is the flipping by 180° of the carbamate moiety. In both cases the carbamate moiety interacts with Arg328, which was already shown to be a binding partner for the carboxylic group of 6ECDCA (Figure 5).[16]

As anticipated above, in chain A, but not in chain B, a third disposition is apparent. This disposition, called complex III, is only achieved by compounds **7e**−**h**, endowed with the largest substituents, and is characterized by a shift of the side chain substituents toward a small cleft situated between loop H1−H2 and loop H5−H6. This cleft is made available by the small conformational rearrangement due to the lack of the second coactivator peptide. It is also interesting to note that at least the other two docking dispositions were identified for individual compounds. Thus, for compound **7b** docked in chain A, a fourth orientation was identified where the cyclohexyl group is more deeply inserted into the additional binding pocket and the steroid skeleton is shifted toward H1−H2. This shift causes the apparent loss of the hydrogen bonds between the 3-OH and 7-OH groups of **7b** and Tyr358 and Tyr366, respectively. Interestingly, however, this loss of H-bond capability does not correspond to a significant decrease in the docking energies, which indeed parallel those of complex I and complex II. When compound **7c** is docked into chain A, another disposition was identified corresponding to a situation in which the large adamantyl group is more clearly pointing toward the protein's surface. In this case, however, the predicted docking energy is significantly lower than that of complex I or II.

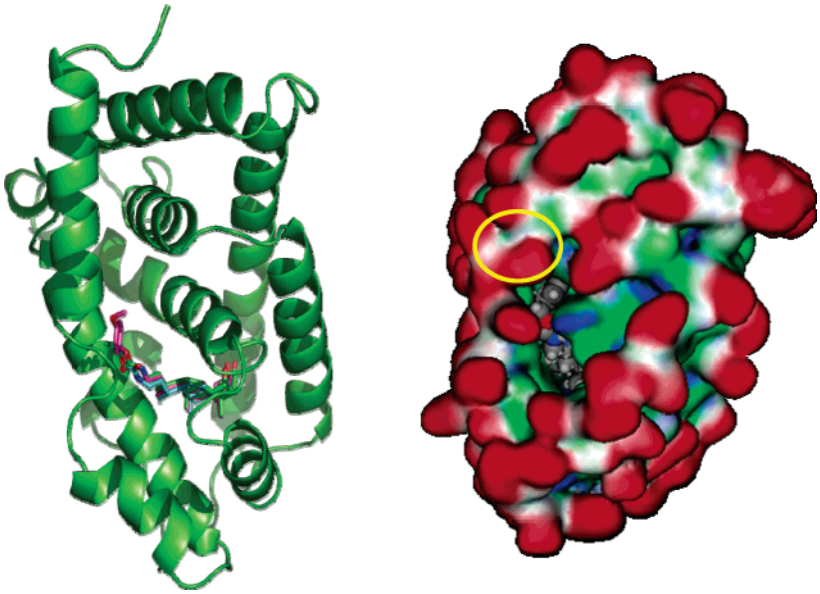

Figure 4. (a) Overall view of the docking results. The crystallographically determined position of 6ECDCA is reported in yellow. The dispositions called complex I, complex II, and complex III are reported in cyan, green, and purple, respectively. (b) Accessible Connolly surface of the LBD of FXR in the same orientation as in Figure 1. The docking pose of compound **7e** (chosen as an example) in its complex I disposition is shown as a space-filled model. It can be appreciated how the additional binding pocket is almost completely filled up by the extended side chain.

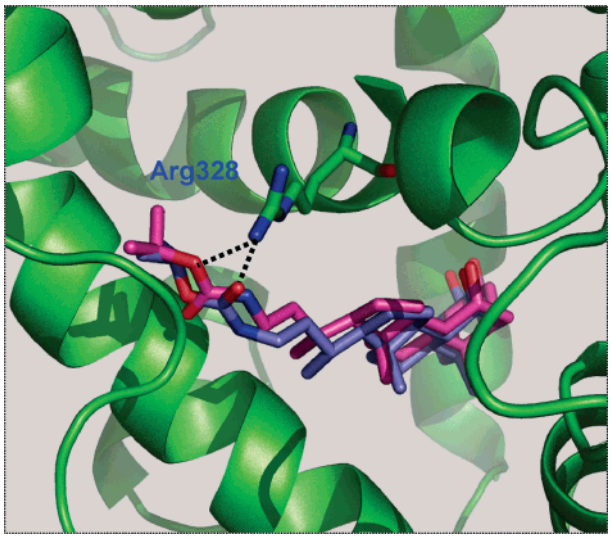

Figure 5. Comparison between complex I and complex II dispositions (compound **7a** is taken as an example). The carbamate moiety is flipped by 180°. As a result, in complex I Arg328 interacts with the carbonyl oxygen atom, while in complex II Arg328 interacts with the carbamic oxygen atom.

Discussion

Substitution of the carboxylic tail of CDCA (**1**) by carbamate moieties resulted in an array of new derivatives (**6**, **7a**−**h**) endowed with high potency as FXR ligands and, interestingly, with a broad range of efficacy in both cell-free FRET and cell-based luciferase assays. The new CDCA analogues are functionalized at the carbamate moiety with a set of diverse alkyl, cycloalkyl, and aromatic rings. Among the newly reported compounds, the thiophene carbamate derivative (**7g**) was shown to be the most potent in the FRET assay. Docking experiments carried out on the crystal structure of the LBD of FXR provided the molecular basis for rationalizing the activity of the new derivatives. In detail, a consistent pattern of docking orientations were identified where the distal substituents are oriented into a newly described additional binding pocket lined by residues belonging to H1, H3, H5. In these docking orientations, the cyclopentanophenanthrene nucleus almost perfectly matched the disposition of the potent agonist 6ECDCA (**4**) in the crystal structure. Comparison of the docking energies with the log EC_{50} values from the FRET experiments indicated a reasonable correlation provided that two outliers (**7f** and **7g**) are eliminated (Figure 6).

In particular, a correlation coefficient (r) of 0.85 and 0.84 is obtained for a set of seven compounds docked in chain A and chain B, respectively. The reason why compound **7f** behaved as an outlier is relatively straightforward, since it is the only compound in the series with a free carboxylate function. This ionized group needs to be desolvated upon binding, and the energy cost of desolvation should be added to the docking energy. More problematic is the explanation for the behavior of **7g**, which bears a thiophene ring and is predicted to be less active than it actually is. The wrong prediction may have to do with inaccuracy of parametrization of the sulfur atom.[23] The good correlation coefficient obtained for the remaining set of compounds constitutes further evidence that all the new derivatives bind FXR in the same orientation and that the variability in potency is modulated basically by the number of hydrophobic contacts that are built-up in the additional binding pocket. When a correlation between docking energies and efficacies is attempted, no significant results could be obtained (results not shown). This suggests that the static picture provided by the docking experiments is not sufficient to explain the ability of the complex receptor−ligand to recruit the coactivator peptide. A dynamic approach will eventually be necessary, and this will be commented further on below.

The new carbamate derivatives have also been tested in a cell-based luciferase assay (Figure 2). Some of the compounds fully transactivate the reporter gene, some resulted in a partial activation, while others, **5**, **7c**, and **7h** in particular, failed to give response. To verify whether this lack of response is due to the compound's inability to cross the cell membrane, a competition experiment was carried out against CDCA (20 μM). The complete abolishment of the CDCA response allowed us to classify compounds **5**, **7c**, and **7h** as pure antagonists in the luciferase assay. Although a broad range of functional response was observed in both the FRET and in the luciferase assays,

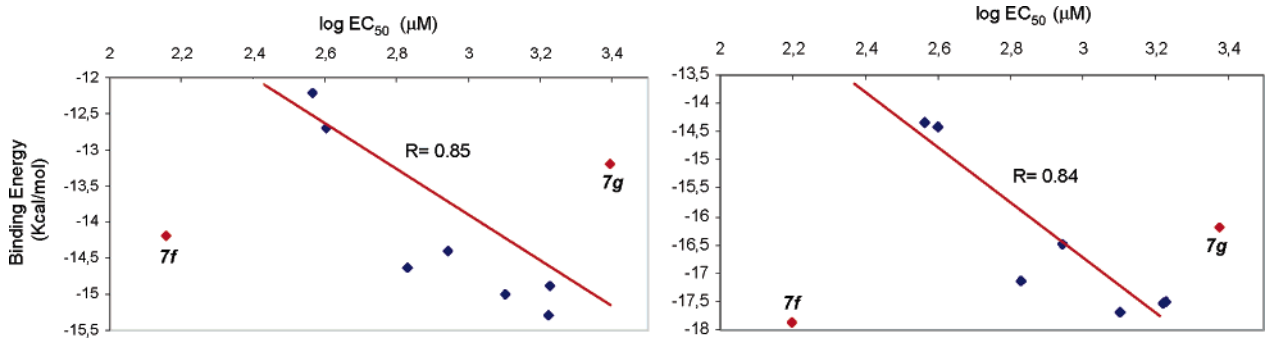

Figure 6. Correlation between Autodock's binding energies and FRET-derived log EC_{50} values. For chain A (left) or in chain B (right), a good correlation could be obtained when two outliers (**7f** and **7g**) are eliminated. See text for explanation.

no correlation could be found between the transactivation data and the FRET efficacy (data not shown). This may reflect the presence, in the cell system, of a variety of coactivator proteins at different concentrations and further confirms that the mechanism of gene expression cannot be linked in a simple and predictable way to the ability to recruit a small peptide in a cell-free assay.

The overall analysis of the FRET and transactivation assays, combined with the docking results, indicated that a broad range of modulation of the functional profile could be attained by chemically modifying the side chains of bile acids. This finding appears to be of particular relevance for two reasons. First, the new derivatives **7a**−**h** represent potentially useful starting points toward the characterization of novel selective FXR modulators. In this regard, selected compounds are being investigated by RT-PCR experiments for their ability to selectively induce (or repress) individual genes in in vivo conditions. The second reason is very intriguing because we demonstrated that it is possible to achieve full agonism, partial agonism, or antagonism by modifying a part of the molecule that is not directly interacting with any of the LBD elements known to affect coactivator binding. Thus, the classical paradigm for nuclear receptor modulation demands a perturbation by the ligand of the mutual disposition of helices H12 and H3 whose "active" orientation allows the correct docking of the coactivator protein and, hence, the consequent gene activation. Modulators of nuclear receptors have been described as agents able to perturb, to various extent, the relative orientations of H12 and H3. In our present case, a broad range of modulation is obtained by chemically modifying a part of the molecules (i.e. the extended side chain) that is predicted to project toward loop H1−H2 without an apparent impact on the conformation of either H12 or H3. The significance of this observation and its possible extension to other members of the nuclear receptor superfamily deserves further investigation, and the static picture provided here by docking analysis is certainly not sufficient to draw a conclusive hypothesis. It is very interesting to observe that the potential for broad modulation endowed with occupancy of "secondary" sites may be exploited by small nonsteroidal ligands that can eventually be designed to be directed toward these sites. It is also interesting to speculate that several independent observations converge in pointing out a functional role for the H1−H2 loop in FXR: (i) bile acids bind FXR upward orientated when compared with other metabolic nuclear receptor endogenous activators; (ii) a second coactivator peptide has been cocrystallized with rFXR docked in a cleft parallel to the H1−H2 loop; (iii) in a recent computational study we have identified so far an unreported cavity in FXR, close to the H1−H2 loop, and we have also proposed that guggulsterone may bind to this pocket.[18]

In conclusion, we provide here the first evidence that the receptor's back door in FXR can be exploited to achieve a broad range of modulation, an observation that may be of great relevance toward the design of selective FXR modulators and that can in principle be extended to other members of the nuclear receptor superfamily.

Experimental Section

Chemistry. Melting points were determined with a Buchi 535 electrothermal apparatus and are uncorrected. NMR spectra were obtained with a Bruker AC 200 or 400 MHz spectrometer, and the chemical shifts are reported in parts per million (ppm). The abbreviations used are as follows: s, singlet; bs, broad singlet; d, doublet; dd, double of a doublet; m, multiplet. Specific rotations were recorded on a Jasco Dip-360 digital polarimeter. Flash column chromatography was performed using Merck silica gel 60 (0.040−0.063 mm). TLC was carried out on precoated TLC plates with silica gel 60 F-254 (Merck). Spots were visualized by staining and warming with phosphomolybdate reagent (5% solution in EtOH). The analytical HPLC measurements were made on a Shimadzu (Kyoto, Japan) LC workstation, class LC-8A, equipped with an SPD-10Avp variable-wavelength UV−visible detector and a Rheodyne 7725i injector with a 20-μL stainless steel loop. The chromatographic traces were obtained with CLASS VP (Shimadzu, version 4.3) software. The UV detection wavelength was set at 205 nm (first detection channel) and at 254 nm (second detection channel). The flow rate was 1.0 mL/min, and all the analyses were performed at room temperature. A LiChrospher 100 RP-18 (Merck (Darmstadt, Germany), 250 mm × 4.0 mm i.d., 5 μm, 100 Å) and an Ultra Aqueous C18 (Restek (Bellefonte, PA), 250 mm × 4.6 mm i.d., 5 μm, 100 Å) were used as analytical columns. All reaction were carried out under a nitrogen atmosphere.

Preparation of Isocyanate Intermediate 9. 3α,7α-Diformyloxy-5β-cholan-24-oic acid (**8**)[21] (6.0 g, 13.37 mmol) was treated with oxalyl chloride (7.0 mL) and reacted at 35 °C for 3 h under nitrogen atmosphere. Removal of oxalyl chloride by evaporation gave the corresponding acyl chloride, which was dissolved in dry acetone (50 mL). A solution of NaN_3 (5.2 g, 80.25 mmol) in water (25 mL) was added to the solution at 0−5 °C, and the resulting reaction mixture was stirred for an additional 3 h at the same temperature. The solvents were removed, and the residue was poured into cold water (100 mL) and extracted with diethyl ether (3 × 100 mL). The combined organic phases were dried over anhydrous Na_2SO_4 and evaporated to obtain the corresponding acyl azide (IR, 2134 and 2267 cm^{-1}). The acyl azide intermediate so obtained was then refluxed in dry toluene (60 mL) for 5 h. The mixture was evaporated under vacuum to give 5.1 g of the isocyanate derivative **9** (11.37 mmol, 85%, IR 2271 cm^{-1}) that was used for the next step without any purification.

Parallel Synthesis of Carbamate Analogues of CDCA (7a−h). With a carousel apparatus, the intermediate isocyanate **9** (1.5 mmol) was dissolved in dry toluene (5 mL) and then reacted with the eight different alcohols (1.2 equiv, Table 3) at 90 °C under nitrogen atmosphere. The end of the reactions was checked by TLC. Each reaction mixture was then poured into water (10 mL). The organic phase was separated, and the aqueous phase was extracted with ethyl acetate (3 × 5 mL). The combined organic phases were

washed with brine, dried (Na_2SO_4), filtered, and concentrated under vacuum. The crude 23-*N*-carboxy-3α,7α-diformyloxy-24-nor-5β-cholan-23-amine derivatives were then treated overnight with a saturated methanolic solution of K_2CO_3 (5 mL) at room temperature. After evaporation of the solvent, the residues were dissolved in water (5 mL), acidified with 2 N HCl, and extracted with dichloromethane (3 × 5 mL). The combined organic extracts were dried over anhydrous Na_2SO_4, filtered, concentrated under vacuum, and purified by silica gel flash chromatography using a mixture of dichloromethane/methanol as eluent, affording the desired compounds in good yields (Table 3).

23-*N*-(Carboisopropyloxy)-3α,7α-dihydroxy-24-nor-5β-cholan-23-amine (7a). Mp: 88−90 °C. ^{1}H NMR ($CDCl_3$) δ: 0.68 (s, 3H, 18-CH_3), 0.92−0.97 (m, 6H, 19-CH_3 and 21-CH_3), 1.16−1.18 (d, 6H, CH(CH_3)$_2$), 3.05−3.42 (m, 2H, 23-CH_2), 3.46−3.50 (m, 1H, 3-CH), 3.87 (m, 1H, 7-CH), 4.51 (bs, 1H, NH), 4.90−4.94 (m, 1H, C*H*(CH_3)$_2$). ^{13}C NMR ($CDCl_3$) δ: 11.63, 18.53, 20.46, 22.09, 22.66, 23.60, 28.21, 30.57, 32.74, 33.69, 34.51, 34.94, 35.21, 36.04, 38.40, 39.32, 39.52, 39.80, 41.37, 42.62, 50.36, 55.92, 67.73, 68.43, 71.91, 156.43.

23-*N*-(Carbocyclohexyloxy)-3α,7α-Dihydroxy-24-nor-5β-cholan-23-amine (7b). Mp: 92−96 °C. ^{1}H NMR ($CDCl_3$) δ: 0.60 (s, 3H, 18-CH_3), 0.92 (s, 3H, 19-CH_3), 0.97−0.99 (d, 3H, 21-CH_3), 3.10−3.12 (m, 1H, 23-CH_2), 3.24−3.28 (m, 1H, 23-CH_2), 3.45−3.52 (m, 1H, 3-CH), 3.86 (s, 1H, 7-CH), 4.62 (br, 1H, NH), 4.65 (bs, 1H, −OC*H*). ^{13}C NMR ($CDCl_3$) δ: 11.63, 18.54, 20.47, 22.67, 23.59, 23.73, 25.34, 28.22, 30.53, 31.96, 32.73, 33.67, 34.49, 34.94, 35.22, 36.07, 38.42, 39.31, 39.52, 39.73, 41.38, 42.62, 50.35, 55.93, 68.42, 71.92, 72.78, 156.43.

23-*N*-(Carbo-2′-adamantyloxy)-3α,7α-dihydroxy-24-nor-5β-cholan-23-amine (7c). Mp: 113−117 °C. ^{1}H NMR ($CDCl_3$) δ: 0.68 (s, 3H, 18-CH_3), 0.92 (s, 3H, 19-CH_3), 0.97−0.99 (d, 3H, 21-CH_3), 3.08−3.24 (m, 1H, 23-CH_2), 3.26−3.31 (m, 1H, 23-CH_2), 3.45−3.52 (m, 1H, 3-CH), 3.85 (m, 1H, 7-CH), 4.62 (bs, 1H, NH), 4.82 (s, 1H, −OCH). ^{13}C NMR ($CDCl_3$) δ: 11.71, 18.67, 20.55, 22.75, 23.68, 27.01, 27.28, 28.32, 30.62, 31.83, 32.11, 32.82, 33.77, 34.59, 35.02, 35.31, 36.34, 37.43, 39.40, 39.61, 39.83, 41.67, 42.70, 50.43, 56.03, 68.50, 72.00, 156.33.

23-*N*-(Carbobenzyloxy)-3α,7α-dihydroxy-24-nor-5β-cholan-23-amine (7d). Mp: 75−79 °C. ^{1}H NMR ($CDCl_3$) δ: 0.67 (s, 3H, 18-CH_3), 0.92 (s, 3H, 19-CH_3), 0.97−0.99 (d, 3H, 21-CH_3), 3.06−3.18 (m, 1H, 23-CH_2), 3.21−3.41 (m, 1H, 23-CH_2), 3.40−3.50 (m, 1H, 3-CH), 3.86 (br, 1H, 7-CH), 4.61−4.72 (bs, 1H, NH), 5.12 (s, 2H, −OCH_2), 7.28−7.38 (m, 3H). ^{13}C NMR ($CDCl_3$) δ: 11.63, 18.49, 20.46, 22.66, 23.59, 28.23, 30.56, 32.73, 33.65, 34.50, 34.94, 35.22, 35.97, 38.59, 39.32, 39.52, 39.79, 41.37, 42.62, 50.35, 55.91, 66.47, 68.42, 71.92, 127.97, 128.41, 136.58, 156.24.

23-*N*-(Carbo-*p*-methoxybenzyloxy)-3α,7α-dihydroxy-24-nor-5β-cholan-23-amine (7e). Mp: 80−83 °C. ^{1}H NMR ($CDCl_3$) δ: 0.65 (s, 3H, 18-CH_3), 0.89 (s, 3H, 19-CH_3), 0.94−0.97 (d, 3H, 21-CH_3), 3.04−3.22 (m, 1H, 23-CH_2), 3.26−3.34 (m, 1H, 23-CH_2), 3.44−3.52 (m, 1H, 3-CH), 3.81 (s, 3H, −OCH_3), 3.85 (m, 1H, 7-CH), 4.59 (bs, 1H, NH), 5.12 (s, 2H, −OCH_2), 6.78−6.92 (d, 2H, Ph), 7.28−7.32 (d, 2H, Ph). ^{13}C NMR ($CDCl_3$) δ: 11.35, 18.50, 20.50, 22.72, 23.61, 28.27, 30.45, 32.73, 33.70, 34.48, 34.98, 35.24, 35.96, 38.47, 39.30, 39.56, 41.39, 42.64, 50.36, 55.24, 55.96, 66.38, 68.38, 71.82, 113.86, 128.68, 129.94, 156.51, 159.47.

23-*N*-(Carbo-*p*-carboxybenzyloxy)-3α,7α-dihydroxy-24-nor-5β-cholan-23-amine (7f). Mp: 120−123 °C. ^{1}H NMR ($CDCl_3$) δ: 0.62 (s, 3H, 18-CH_3), 0.89 (s, 3H, 19-CH_3), 0.93−0.96 (d, 3H, 21-CH_3), 3.02−3.22 (m, 1H, 23-CH_2), 3.23−3.33 (m, 1H, 23-CH_2), 3.40−3.50 (m, 1H, 3-CH), 3.84 (m, 1H, 7-CH), 4.89 (bs, 1H, NH), 5.15 (s, 2H, −OCH_2), 7.39−7.43 (d, 2H, Ph), 8.04−8.08 (d, 2H, Ph). ^{13}C NMR ($CDCl_3$) δ: 11.65, 18.57, 20.51, 22.73, 23.59, 28.33, 30.39, 32.76, 33.73, 34.47, 34.98, 35.25, 35.95, 38.66, 39.31, 39.54, 41.40, 42.65, 50.35, 55.88, 65.72, 68.48, 72.00, 127.44, 129.27, 130.29, 142.41, 156.15, 169.89.

23-*N*-(Carbothiophene-2′-methyloxy)-3α,7α-dihydroxy-24-nor-5β-cholan-23-amine (7g). Mp: 87−90 °C. ^{1}H NMR ($CDCl_3$) δ: 0.54 (s, 3H, 18-CH_3), 0.79 (s, 3H, 19-CH_3), 0.82−0.85 (d, 3H, 21-CH_3), 2.89−3.26 (m, 2H, 23-CH_2), 3.26−3.45 (m, 1H, 3-CH), 3.71−3.73 (br, 1H, 7-CH), 4.56 (bs, 1H, NH), 5.13 (s, 2H, −OCH_2), 6.85−6.89 (dd, 1H), 6.97−6.99 (dd, 1H), 7.18−7.21 (dd, 1H). ^{13}C NMR ($CDCl_3$) δ: 11.63, 18.52, 20.46, 22.66, 23.58, 28.24, 30.50, 32.73, 33.67, 34.47, 35.21, 36.01, 38.59, 39.30, 39.51, 39.70, 41.36, 42.62, 50.33, 55.91, 60.80, 68.41, 71.92, 126.64, 126.79, 129.69, 138.72, 156.00.

23-*N*-(Carbocinnamyloxy)-3α,7α-dihydroxy-24-nor-5β-cholan-23-amine (7h). Mp: 79−84 °C. ^{1}H NMR ($CDCl_3$) δ: 0.67 (s, 3H, 18-CH_3), 0.92 (s, 3H, 19-CH_3), 0.98−0.99 (d, 3H, 21-CH_3), 3.09−3.22 (m, 1H, 23-CH_2), 3.23−3.31 (m, 1H, 23-CH_2), 3.46−3.57 (m, 1H, 3-CH), 3.86 (s, 1H, 7-CH), 4.73−4.74 (d, 2H, −OC*H*$_2$CH), 6.28−6.35 (m, 1H, −OCH$_2$C*H*), 6.63−6.68 (d, 1H, −C*H*Ph), 7.25−7.41 (m, 5H, Ph). ^{13}C NMR ($CDCl_3$) δ: 11.64, 18.52, 20.46, 22.66, 23.58, 28.24, 30.50, 32.73, 33.67, 34.47, 34.94, 35.21, 36.08, 38.59, 39.30, 39.51, 39.70, 41.36, 42.62, 50.34, 55.91, 65.20, 68.41, 71.92, 123.96, 126.49, 127.83, 128.46, 133.47, 136.28, 153.43.

Biology. Compounds were assayed by fluorescence resonance energy transfer for recruitment of the SRC-1 peptide to human FXR using a cell-free LiSA as described elsewere.[6]

HepG2 cells were cultured in E-MEM supplemented with 1% penicillin/streptomycin, 1% l-glutamine, and 10% fetal bovine serum (high glucose) (Invitrogen, Carlsbad, CA). Cells were grown at 37 °C in 5% CO_2. All the transfections were done using a calcium phosphate coprecipitation method in the presence of 25 μM chloroquine as inhibitor for DNA degradation. Twenty-four hours before transfection, HepG2 cells were seeded onto a six-well plate at a density of 400 000 cells/well. Transient transfections were performed using 500 ng of reporter vector pHSP27-TK-Luc containing the FXR response element (FXRE), 200 ng of pCMV-βgal, as internal control for transfection efficiency, and 50 ng of each receptor expression plasmid pSG5-FXR, pSG5-RXR. The pGEM vector was added to normalize the amounts of DNA transfected in each assay (2.5 μg). At 36−48 h post-transfection, the cells were stimulated with CDCA (control ligand), **5**, **6**, and **7a**−**h** at 20 μM for 18 h, all diluted in DMSO. Control cultures received vehicle (0.1% DMSO) alone. The cells were lysed in 100 μL of diluted reporter lysis buffer (Promega), and 10 μL (HepG2) of cellular lisates was assayed for luciferase activity using the luciferase assay system (Promega). Luminescence was measured using an automated luminometer. Luciferase activities were normalized for transfection efficiencies by dividing the relative light units by β-galactosidase activity expressed from cotransfected pCMV-βgal plasmid. Each data point is the average of triplicate assays. Each experiment was repeated almost three times.

Molecular Modeling. Preparation of Ligands. Ligands were built and optimized using the Sybyl program[24] by using the geometry of 6ECDCA in the crystal structure as the starting point. Thus, the ligand was extracted from the complex, the atom and bond types were carefully checked, the 6α-ethyl group was deleted, and appropriate fragments from the Sybyl libraries were used to build each new molecule. After the addition of hydrogen atoms Gasteiger−Marsili partial atomic charges were calculated[25] and every molecule was optimized until the energy gradient was smaller than 0.05 kcal·mol^{-1}·Å^{-2}. The optimized molecules were saved in mol2 format and used for the preparation of the pdbq file employed by Autodock.[26] ADT program[27] was used to read the molecule, delete the nonpolar hydrogen atoms, define the anchor atom and the rotatable bonds and write the pdbq file.

Preparation of the Receptor. The ADT program[27] was used to prepare the receptor for the docking study. Thus, chain B of the crystal structure of the FXR/6ECDCA complex was extracted and imported into the ADT program; polar hydrogen, partial atomic charges, and solvation parameters were added, and the file pdbqs was written in order to generate the potential maps needed for the docking calculations.

Docking Procedure. Potential maps were generated using the AUTOGRID program, available in the Autodock package, using a grid centered in the 6ECDCA binding pocket with a size of 80 points × 74 points × 70 points and a grid spacing 0.375 Å. The 200 runs of GA were carried out for each ligand using the standard conditions defined in the Autodock program. Final geometries of

each run were compared with the initial geometry and clustered as a function of its free energy of binding. Table 2 summarizes the total number of clusters found for each compound, the order (binding energy) of the more populated cluster, the number of conformations in the more populated cluster, and the docking and binding energiesy of the more favored conformation of the more populated cluster. In general, the more populated cluster is also the more stable one. For compounds **7a** and **7c** only, the more populated cluster is the second one in energy, but the difference in the free energy of binding is smaller than 0.5 kcal/mol. In compound **7b**, there is also a second highly populated cluster with a binding energy similar to that of the more stable (and populated) one. In general, more than a 50% of the conformations belong to the more populated cluster.

Acknowledgment. Timothy M. Willson (GlaxoSmithKline, R&D, Research Triangle Park, NC) and Dr. Mark Pruzanski (Intercept Pharmaceuticals) are acknowledged for useful discussions. Intercept Pharmaceutical is gratefully acknowledged for financial support and Erregierre (Bergamo, Italy) for the gift of bile acids as starting material.

Supporting Information Available: Elemental analysis, HPLC traces, and thin-layer chromatography plates of all target compounds. This material is available free of charge via the Internet at http://pubs.acs.org.

References

(1) Pellicciari, R.; Costantino, G.; Fiorucci, S. Farnesoid X receptor: from structure to potential clinical applications *J. Med. Chem.* **2005**, *48*, 5383−5403.
(2) Wang, H.; Chen, J.; Hollister, K.; Sowers, L. C.; Forman, B. M. Endogenous bile acids are ligands for the nuclear receptor FXR/BAR. *Mol. Cell* **1999**, *3*, 543−553.
(3) Parks, D. J.; Blanchard, S. G.; Bledsoe, R. K.; Chandra, G.; Consler, T. G.; Kliewer, S. A.; Stimmel, J. B.; Willson, T. M.; Zavacki, A. M.; Moore, D. D.; Lehmann, J. M. Bile acids: natural ligands for an orphan nuclear receptor. *Science* **1999**, *284*, 1365−1368.
(4) Makishima, M.; Okamoto, A. Y.; Repa, J. J.; Tu, H.; Learned, R. M.; Luk, A.; Hull, M. V.; Lustig, K. D.; Mangelsdorf, D. J.; Shan, B. Identification of a nuclear receptor for bile acids. *Science* **1999**, *284*, 1362−1365.
(5) Pellicciari, R.; Fiorucci, S.; Camaioni, E.; Clerici, C.; Costantino, G.; Maloney, P. R.; Morelli, A.; Parks, D. J.; Willson, T. M. 6-α-Ethyl-chenodeoxycholic acid (6-ECDCA), a potent and selective FXR agonist endowed with anticholestatic activity. *J. Med. Chem*. **2002**, *45*, 3569−3572.
(6) Maloney, P. R.; Parks, D. J.; Haffner, C. D.; Fivush, A. M.; Chandra, G.; Plunket, K. D.; Creech, K. L.; Moore, L. B.; Wilson, J. G.; Lewis, M. C.; Jones, S. A.; Willson, T. M. Identification of a chemical tool for the orphan nuclear receptor FXR. *J. Med. Chem*. **2000**, *43*, 2971−2974.
(7) Nicolaou, K. C.; Evans, R. M.; Roecker, A. J.; Hughes, R.; Downes, M.; Pfefferkorn, J. A. Discovery and optimization of non-steroidal FXR agonists from natural product-like libraries. *Org. Biomol. Chem.* **2003**, *1*, 908−920.
(8) Goodwin, B.; Jones, S. A.; Price, R. R.; Watson, M. A.; McKee, D. D.; Moore, L. B.; Galardi, C.; Wilson, J. G.; Lewis, M. C.; Roth, M. E.; Maloney, P. R.; Willson, T. M.; Kliewer, S. A. A regulatory cascade of the nuclear receptors FXR, SHP-1, and LRH-1 represses bile acid biosynthesis. *Mol. Cell* **2000**, *6*, 517−526.
(9) Lu, T. T.; Makishima, M.; Repa, J. J.; Schoonjans, K.; Kerr, T. A.; Auwerx, J.; Mangelsdorf, D. J. Molecular basis for feedback regulation of bile acid synthesis by nuclear receptors. *Mol. Cell* **2000**, *6*, 507−515.
(10) Denson, L. A.; Sturm, E.; Echaverria, W.; Zimmerman, T. L.; Makishima, M.; Mangelsdorf, D. J.; Karpen, S. J. The orphan nuclear receptor shp mediates bile acid-induced inhibition of the rat bile acid transporter ntcp. *Gastroenterology* **2001**, *121*, 140−147.
(11) Sinal, C. J.; Tohkin, M.; Miyata, M.; Ward, J. M.; Lambert, G.; Gonzales, F. J. Targeted disruption of the nuclear receptor FXR/BAR impairs bile acid and lipid homeostasis. *Cell* **2000**, *102*, 731−744.
(12) Duran-Sandoval, D.; Mautino, G.; Martin, G.; Percevault, F.; Barbier, O.; Fruchart, J. C.; Kuipers, F.; Staels, B. Glucose regulates the expression of the farnesoid X receptor in liver. *Diabetes* **2004**, *53*, 890−898.
(13) Stayrook, K. R.; Bramlett, K. S.; Savkur, R. S.; Ficorilli, J.; Todd, C.; Christe, M. E.; Michael, L. F.; Burris, T. P. Regulation of carbohydrate metabolism by the farnesoid X receptor. *Endocrinology* **2005**, *146*, 984−991.
(14) Duran-Sandoval, D.; Cariou, B.; Fruchart, J.-C.; Staels, B. Potential regulatory role of the farnesoid X receptor in the metabolic syndrome. *Biochimie* **2005**, *87*, 93−98.
(15) Wurtz, J. M.; Bourguet, W.; Renaud, J. P.; Vivat, V.; Chambon, P.; Moras, D.; Gronemeyer, H. A canonical structure for the ligand-binding domain of nuclear receptors. *Nat. Struct. Biol.* **1996**, *3*, 87−94.
(16) Mi, L. Z.; Devarakonda, S.; Harp, J. M.; Han, Q.; Pellicciari, R.; Willson, T. M.; Khorasanizadeh, S.; Rastinejad, F. Structural basis for bile acid binding and activation of the nuclear receptor FXR. *Mol. Cell* **2003**, *11*, 1093−1100.
(17) (a) Bledsoe, R. K.; Montana, V. G.; Stanley, T. B.; Delves, C. J.; Apolito, C. J.; McKee, D. D.; Consler, T. G.; Parks, D. J.; Stewart, E. L.; Willson, T. M.; Williams, S. P. A ligand-mediated hydrogen bond network required for the activation of the mineralocorticoid receptor. *Cell* **2002**, *110*, 93−105. (b) Brzozowski, A. M.; Pike, A. C.; Dauter, Z.; Hubbard, R. E.; Bonn, T.; Engstrom, O.; Ohman, L.; Greene, G. L.; Gustafsson, J. A.; Carlquist, M. Molecular basis of agonism and antagonism in estrogen receptor. *Nature* **1997**, *389*, 753−758. (c) Sack, J. S.; Kish, K. F.; Wang, C.; Attar, R. M.; Kiefer, S. E.; An, Y.; Wu, G. Y.; Scheffler, J. E.; Salvati, M. E.; Krystek, S. R.; et al. Crystallographic structures of the ligand-binding domains of the androgen receptor and its T877A mutant complexed with the natural agonist dihydrotestosterone. *Proc. Natl. Acad. Sci. U.S.A.* **2001**, *98*, 4904−4909. (d) Shiau, A. K.; Barstad, D.; Loria, P. M.; Cheng, L.; Kushner, P. J.; Agard, D. A.; Greene, G. L. The structural basis of estrogen receptor/coactivator recognition and the antagonism of this interaction by tamoxifen. *Cell* **1998**, *95*, 927−937. (e) Williams, S. P.; Sigler, P. B. Atomic structure of progesterone complexed with its receptor. *Nature* **1998**, *393*, 392−396.
(18) Meyer, U.; Costantino, G.; Macchiarulo, A.; Pellicciari, R. Is antagonism of *E*/*Z*-guggulsterone at the farnesoid X receptor mediated by a noncanonical binding site? A molecular modeling study. *J. Med. Chem.* **2005**, *48*, 6948−6955.
(19) Pellicciari, R.; Costantino, G.; Camaioni, E.; Sadeghpour, B. M.; Entrena, A.; Willson, T. M.; Fiorucci, S.; Clerici, C.; Gioiello, A. Bile acid derivatives as ligands of the farnesoid X receptor. Synthesis, evaluation, and structure−activity relationship of a series of body and side chain modified analogues of chenodeoxycholic acid. *J. Med. Chem.* **2004**, *47*, 4559−4569.
(20) Coleman, J. P.; Kirby, L. C.; Setchell, K. D.; Hylemon, P. B.; Pandak, M.; Heuman, D. M.; Vlahcevic, Z. R. Metabolic fate and hepatocyte toxicity of reverse amide analogs of conjugated ursodeoxycholate in the rat. *J. Steroid Biochem. Mol. Biol.* **1998**, *64*, 91−101.
(21) Goto, J.; Kato, H.; Hasegawa, F.; Nambara, T. Synthesis of monosulfates of unconjugated bile acids. *Chem. Pharm. Bull.* **1979**, *27*, 1402−1411.
(22) Costantino, G.; Entrena-Gaudix, A.; Macchiarlo, A.; Gioiello, A.; Pellicciari, R. Molecular dynamics simulation of the ligand binding domain of farnesoid X receptor. Insight into helix-12 stability and coactivator peptide stabilization in response to agonist binding. *J. Med. Chem.* **2005**, *48*, 3251−3259.
(23) Olsen, L.; Pettersson, I.; Hemmingsen, L.; Adolph, H. W.; Jorgensen, F. S. Docking and scoring of metallo-beta-lactamases inhibitors. *J. Comput.-Aided Mol. Des.* **2004**, 18, 287−302
(24) *Sybyl Molecular Modeling Software*; Tripos Inc. (1699 S. Hanley Rd, St. Louis, MO 63144-2913); http://www.tripos.com.
(25) (a) Gasteiger, J.; Marsili, M. Iterative partial equalization of orbital electronegativity. A rapid access to atomic charges. *Tetrahedron*, **1980**, *36*, 3219−3228. (b) Marsili, M.; Gasteiger, J. Charge distributions from molecular topology and pi-orbital electronegativity. *Croat. Chem. Acta* **1980**, *53*, 601−614. (c) Gasteiger, J.; Marsili, M. Prediction of proton magnetic resonance shifts: the dependence on hydrogen charges obtained by iterative partial equalization of orbital electronegativity. *Org. Magn. Reson.* **1981**, *15*, 353−360.
(26) Morris, G. M.; Goodsell, D. S.; Halliday, R. S.; Huey, R.; Hart, W. E.; Belew, R. K.; Olson, A. J. Automated docking using a Lamarckian genetic algorithm and an empirical binding free energy function. *J. Comput. Chem.* **1998**, *19*, 1639−1662.
(27) AutoDock Tools (ADT) program is available from the Molecular Graphics Laboratory, at The Scripps Research Institute; http://www.scripps.edu/mb/olson/index.html.

JM060294K